CHEMICAL PHYSICS

Rovibrational quantum state resolution of the C_{60} fullerene

P. Bryan Changala[1]*, Marissa L. Weichman[1], Kevin F. Lee[2], Martin E. Fermann[2], Jun Ye[1]*

The unique physical properties of buckminsterfullerene, C_{60}, have attracted intense research activity since its original discovery. Total quantum state–resolved spectroscopy of isolated C_{60} molecules has been of particularly long-standing interest. Such observations have, to date, been unsuccessful owing to the difficulty in preparing cold, gas-phase C_{60} in sufficiently high densities. Here we report high-resolution infrared absorption spectroscopy of C_{60} in the 8.5-micron spectral region (1180 to 1190 wave number). A combination of cryogenic buffer-gas cooling and cavity-enhanced direct frequency comb spectroscopy has enabled the observation of quantum state–resolved rovibrational transitions. Characteristic nuclear spin statistical intensity patterns confirm the indistinguishability of the 60 carbon-12 atoms, while rovibrational fine structure encodes further details of the molecule's rare icosahedral symmetry.

Understanding molecules as quantum mechanical systems is a central objective of chemical and molecular physics. The complex internal dynamics of these systems evolve over wide energy and time scales, as exhibited by the various electronic, vibrational, rotational, and spin degrees of freedom. Polyatomic molecules, in particular, offer the prospect of probing many-body physics in strongly interacting systems. The most comprehensive characterization of a molecular Hamiltonian, which governs intramolecular dynamics, is provided with high-resolution spectroscopy. When a polyatomic molecule is sufficiently cold to concentrate the population into, and thereby spectrally probe, a single rovibrational state, we achieve the unimolecular equivalent of a pure quantum state at absolute zero in the rest frame of the molecule. The precise measurement of transition energies between individual molecular eigenstates yields detailed information about strong, multibody interactions between atoms in a unimolecular polyatomic lattice, thus providing profound insights into complex molecular structure and ensuing interaction dynamics.

Here we report a rotationally resolved spectrum of the 8.5-μm vibrational band of buckminsterfullerene, C_{60}. Following the discovery of C_{60} by Kroto *et al.* in 1985 (*1*), infrared (IR) and ^{13}C nuclear magnetic resonance spectroscopy confirmed its caged, icosahedral structure (*2*–*7*). Subsequent spectroscopic and analytical techniques, including x-ray and electron diffraction (*8*, *9*), optical Raman and neutron scattering (*10*–*15*), matrix isolation IR spectroscopy [see (*16*–*18*) and references therein], and photoelectron spectroscopy (*19*, *20*), have greatly advanced our understanding of this unique molecule. Spectroscopy has also played a central role in the astronomical detection of C_{60} and its derivatives (*21*, *22*). High-resolution IR absorption measurements may help resolve current uncertainties regarding the physical state of astronomical C_{60} (*18*). However, to date, there have been no reports of rovibrational quantum state–resolved measurements of C_{60} molecules. The experiments reported here thus establish C_{60} as the largest molecule, and the only example of rare icosahedral symmetry, for which a complete internal quantum state–resolved spectrum has been observed.

Although quantum state–resolved rovibrational spectroscopy is routine for small, light molecules, systems as large and heavy as C_{60} are much less amenable to high-resolution characterization owing to several intrinsic and technical challenges. The increase in both the number of vibrational modes and the magnitude of the moment of inertia for every additional atom results in considerably more rotation-vibration states populated at a given internal temperature. Rovibrational states excited by an IR photon may be strongly coupled to a highly congested manifold of background dark states, the density of which grows rapidly with increasing internal energy, leading to intramolecular vibrational redistribution (IVR) (*23*). The Doppler broadening of optical transitions due to finite translational temperature serves only to exacerbate this spectral congestion. Furthermore, the low gas-phase densities achievable for heavy, nonvolatile species require high detection sensitivity.

These various experimental challenges are addressed by cooling the translational and internal temperatures of gas-phase molecular samples and probing them at lower internal energy with longer wavelength light. The method of cryogenic buffer-gas cooling is particularly effective for large, heavy molecules (*24*, *25*). We have recently demonstrated the integration of a buffer-gas cooling source with cavity-enhanced direct frequency comb spectroscopy (CE-DFCS) in the mid-IR (*26*, *27*), which enables sensitive, broadband, high-resolution absorption measurements (*28*, *29*). We have since made substantial changes to the buffer-gas cooling conditions to permit the preparation and detection of cold, gas-phase samples of even heavier molecules and have extended the spectral window of this apparatus to the long-wave IR (LWIR) region (*30*). We have targeted the 8.5-μm vibrational band because it is the lowest-energy IR active mode that falls within our accessible wavelength region.

Figure 1A depicts a simplified view of the apparatus used for C_{60} cooling and spectroscopy. A 950 K copper oven sublimates solid C_{60} samples, generating gas-phase molecules with an average internal energy of 6 to 8 eV per molecule populating 10^{26} to 10^{30} vibrational quantum states, as shown in Fig. 1B. These hot molecules flow into a cell anchored to a cryogenic cold finger, where they are thermalized close to the cell-wall temperature via collisions with cold buffer-gas atoms introduced through an annular slit inlet plate surrounding the cell entrance aperture. We interrogate the cold gas-phase molecules with CE-DFCS by coupling a frequency comb into a high-finesse optical cavity surrounding the cold cell, which enhances the absorption signal by a factor on the order of the cavity finesse (F = 6000). The LWIR frequency comb light centered near 8.5 μm is produced by difference frequency generation (DFG) with two near-IR frequency combs originating from a single mode-locked fiber laser (*31*). The comb contains narrow teeth at optical frequencies $\nu_m = m \times f_{rep} + f_0$, where m is the integer mode index, f_{rep} is the repetition rate, and the offset frequency f_0 can be introduced via an external acousto-optic modulator before the difference frequency step. The intensity of each comb tooth transmitted through the cavity is read out using a broadband scanning-arm Fourier transform interferometer (*32*, *33*). Additional experimental details are provided in the materials and methods (*34*).

Our first attempts at observing cold gas-phase C_{60} with low-pressure helium buffer gas conditions similar to our previous work (*26*, *27*) yielded no detectable absorption. However, when the vacuum chamber was flooded with a high pressure of helium buffer gas, a single broad, unresolved absorption feature appeared, as shown by the red trace in Fig. 2A. We attribute this spectrum to partially cooled C_{60} molecules that remain warm enough to occupy many vibrational quantum states. This is not surprising: As can be seen in Fig. 1B, even at room temperature, the vibrational partition function is greater than 10^3. This finding suggested that both a higher number of collisions and more-efficient energy transfer per collision would be required to thermalize C_{60} to its ground vibrational state (*35*). Indeed, we ultimately produced a sufficiently dense, cold C_{60} sample by (i) increasing the buffer-gas mass by switching from helium to argon and (ii) carefully optimizing the buffer-gas flow and oven positioning relative to the inlet slit. The spectrum acquired at these conditions is shown by the blue trace in Fig. 2A and exhibits well-resolved rovibrational fine structure, with

[1]JILA, National Institute of Standards and Technology and University of Colorado, Department of Physics, University of Colorado, Boulder, CO 80309, USA. [2]IMRA America, Inc., Ann Arbor, MI 48105, USA.
*Corresponding author. Email: bryan.changala@colorado.edu (P.B.C.); ye@jila.colorado.edu (J.Y.)

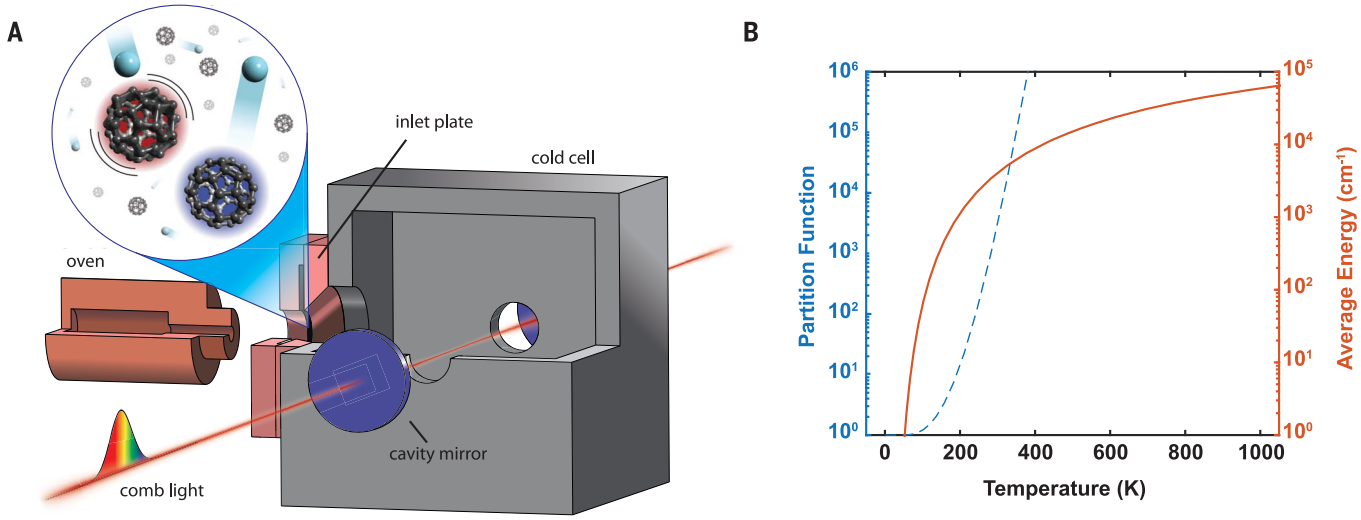

Fig. 1. Cooling and comb spectroscopy of gas-phase C_{60}. (**A**) Sublimated C_{60} vapor exits the oven source and enters a cryogenic cell, where it thermalizes via collisions with cold buffer gas introduced through an annular slit inlet plate surrounding the entrance aperture (see enlarged area). Mid-IR frequency comb light is coupled to an optical enhancement cavity surrounding the cell. The optical absorption spectrum is measured with a scanning arm Fourier transform spectrometer (not pictured). (**B**) The vibrational partition function (blue dashed line) and average vibrational energy (red solid line) increase strongly as a function of temperature. About 6 to 8 eV of vibrational energy must be removed per molecule to cool C_{60} from the initial oven temperature to below 150 K, at which point the vibrational partition function is approximately equal to unity.

narrow linewidths on the order of 20 MHz (fig. S1). The peak absorption, near the band origin, is 10% of the cavity-transmitted comb mode intensity. From the magnitude of the integrated absorption cross section (*17*), we estimate the number density of cold C_{60} to be 4×10^{11} cm^{-3}. Observing the appearance and evolution between the broad and narrow signals was greatly facilitated by the wide spectral bandwidth of the frequency comb, which covers the entire breadth of the observed vibrational band. The inferred rotational temperature is about 150 K (*34*), nearly equal to the cell-wall temperature of 135 K, which is kept well above argon's condensation point of 87 K.

The observed fine structure in the infrared spectrum encodes fundamental details of the quantum mechanical structure of C_{60}. To the zeroth order, the rotations of C_{60} can be considered as those of a spherical top with total angular momentum operator $\mathbf{J}$ (*36*). The associated rotational quantum states are $|J, k, m\rangle$, where J = 0, 1, 2, ... is the total angular momentum quantum number and k, m = $-J$, ..., $+J$ are the projection quantum numbers of the body-fixed component (J_z) and lab-fixed component (J_Z) of $\mathbf{J}$, respectively. The triply degenerate vibrational mode of T_{1u} symmetry that gives rise to the infrared band can be modeled as a three-dimensional isotropic harmonic oscillator with vibrational angular momentum operator $\boldsymbol{\ell}$. Its quantum states are $|n, \ell, k_\ell\rangle$, where n is the total number of vibrational quanta; $\ell = n, n-2, n-4, \ldots$ is the vibrational angular momentum quantum number; and $k_\ell = -\ell, \ldots, +\ell$ is the projection quantum number of the body-frame projection (ℓ_z) of ℓ.

The uncoupled rovibrational product wavefunctions $|J, k, m\rangle|n, \ell, k_\ell\rangle$ are simultaneously eigenfunctions of $\mathbf{J}^2, \ell^2, J_z, \ell_z$, and J_Z. It is useful to define the "pure rotational" angular momentum $\mathbf{R} = \mathbf{J} - \boldsymbol{\ell}$, the eigenfunctions of which can be constructed by transforming the uncoupled product wavefunctions using standard angular momentum coupling relations (*36*). This yields total coupled rovibrational wavefunctions of the form $|R, k_R, J, \ell, n, m\rangle$, where R is the angular momentum quantum number of $\mathbf{R}$ and k_R = $-R$, ..., $+R$ is the body-fixed projection. As usual, the values of R satisfy the triangle inequality $R = |J - \ell|, \ldots, J + \ell$. In this work, we are concerned only with the ground vibrational state with $n = \ell = 0$ and the excited T_{1u} vibrational state, populated by the IR photon, with $n = \ell = 1$. Therefore, in the ground vibrational state, $R = J$; similarly, in the excited state where $\ell = 1$, R is restricted to $J, |J \pm 1|$.

The energies of the states we observe are determined by effective rotational Hamiltonians for each vibrational state. The simplest possible effective Hamiltonian for the ground vibrational state is that of a rigid spherical top

$$H_{\mathrm{gr}} = B''\mathbf{J}^2 \qquad (1)$$

where B'' is the ground state rotational constant, which is inversely proportional to the moment of inertia. The ground state wavefunctions $|R = J, k_R, J, \ell = 0, n = 0, m\rangle$ are eigenstates of H_{gr} with energies

$$E_{\mathrm{gr}} = B''J(J+1) \qquad (2)$$

This energy is independent of k_R and m, leading to the usual $(2R + 1)(2J + 1) = (2J + 1)^2$ spherical-top ground-state degeneracy factor.

Table 1. Fitted spectroscopic parameters of Eq. 6 for the R branch. The residuals (Fig. 4B) have a small root-mean-square error of 7.4×10^{-5} cm^{-1}, slightly larger than the 1σ line-center measurement uncertainty of 2.5×10^{-5} cm^{-1}.

Parameter	Value (cm^{-1})
$\nu_0 + (2\bar{B} + \Delta B)(1 - 2\zeta)$	1184.86196(3)
$2\bar{B}(1 - \zeta) + \Delta B(2 - \zeta)$	0.0078300(3)
ΔB	$-2.876(6) \times 10^{-7}$

The excited vibrational state is described to lowest order by a slightly more sophisticated effective Hamiltonian,

$$H_{\mathrm{ex}} = \nu_0 + B'\mathbf{J}^2 - 2B'\zeta(\mathbf{J} \cdot \boldsymbol{\ell}) \qquad (3)$$

where ν_0 is the vibrational band origin, and B' is the excited state rotational constant, which differs slightly from B'' owing to changes of the moment of inertia upon vibrational excitation. The new rightmost term arises from Coriolis forces that couple the total angular momentum $\mathbf{J}$ and the vibrational angular momentum $\boldsymbol{\ell}$, with $\ell = 1$. The ζ constant encodes the strength of this coupling, which is determined by the geometric details of the vibrational normal mode. The excited state wavefunctions $|R, k_R, J, \ell = 1, n = 1, m\rangle$ are eigenstates of H_{ex} with energy levels at

$$E_{\mathrm{ex}} = \nu_0 + B'J(J+1) - B'\zeta[J(J+1) + \ell(\ell+1) - R(R+1)] \qquad (4)$$

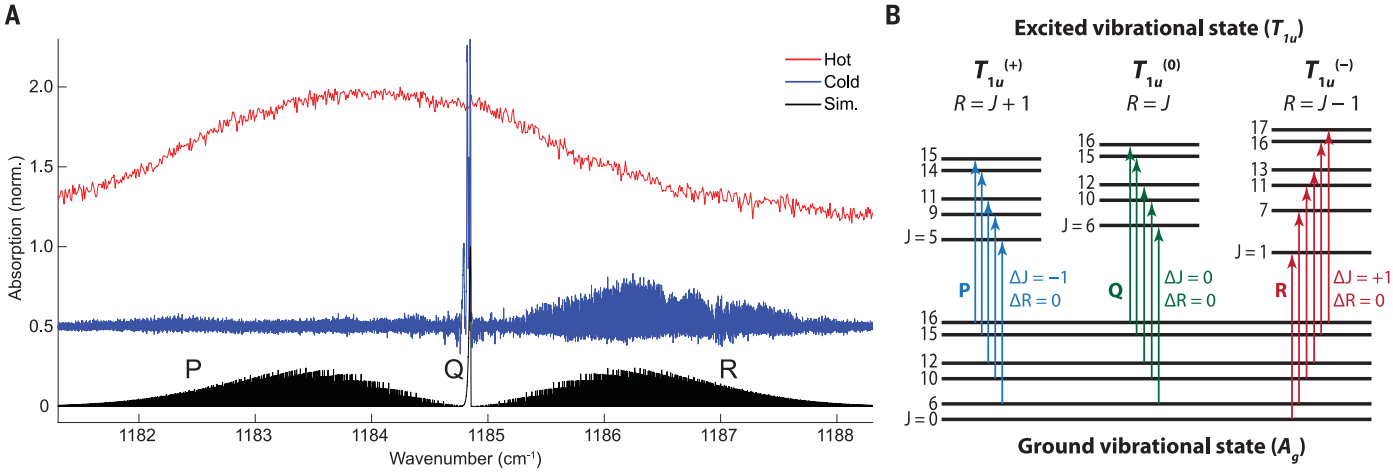

Fig. 2. Spectroscopic patterns of the IR active vibrational band of $^{12}C_{60}$ near 8.5 μm. (**A**) A simulated (sim.) spectrum (black trace) is compared to a measured spectrum of cold (blue trace) and hot (red trace) C_{60}. The measured hot spectrum shows broad, unresolved absorption owing to many thermally occupied vibrational states. The cold spectrum exhibits sharp, well-resolved rotational structure from transitions out of the ground vibrational state. norm., normalized to peak absorption. (**B**) Rovibrational transitions between the ground vibrational state and the excited state follow zeroth-order selection rules of $\Delta J = 0, \pm 1$ and $\Delta R = 0$. These lead to independent P ($\Delta J = -1$), Q ($\Delta J = 0$), and R ($\Delta J = +1$) branches that access the upper-state manifolds labeled $T_{1u}^{(+)}$ (for $R = J + 1$), $T_{1u}^{(0)}$ (for $R = J$), and $T_{1u}^{(-)}$ (for $R = J - 1$), respectively.

again with a degeneracy of $(2R + 1)(2J + 1)$. As $R = J, |J \pm 1|$, the excited state energies sort into three distinct manifolds (*37*)

$$\begin{aligned} E_{ex}^{(+)} &= E_J + 2B'\zeta J, & R &= J + 1 \\ E_{ex}^{(0)} &= E_J - 2B'\zeta, & R &= J \\ E_{ex}^{(-)} &= E_J - 2B'\zeta(J + 1), & R &= J - 1 \end{aligned} \quad (5)$$

where $E_J = \nu_0 + B'J(J + 1)$ is the pure vibrational and rigid rotor contribution to the energy. Physically, these manifolds correspond to states where **J** and $\boldsymbol{\ell}$ are mutually antiparallel, perpendicular, and parallel, respectively.

Rovibrational transitions between the ground and excited T_{1u} vibrational states of spherical tops such as C_{60} are governed by the usual strict $\Delta J = 0, \pm 1$ rule and an additional $\Delta R = \Delta k_R = 0$ rule (*36*). These allowed transitions are illustrated in the level diagram of Fig. 2B. Unlike less symmetric molecules, these selection rules dictate that the usual P ($\Delta J = -1$), Q ($\Delta J = 0$), and R ($\Delta J = +1$) transitions reach mutually exclusive sets of upper state quantum levels. These three manifolds are labeled $T_{1u}^{(+)}$, $T_{1u}^{(0)}$, and $T_{1u}^{(-)}$, according to the energy expressions in Eq. 5.

Inspection of the level diagram in Fig. 2B shows that states with certain values of R are missing. This is, in fact, an exceptional example of nuclear spin statistics at work. The carbon nuclei in pure $^{12}C_{60}$ are each identical spin-0 bosons, so any permutation of nuclei must leave the total molecular wavefunction unchanged. This imposes the strict condition that only states with a total rovibronic symmetry of A_g (+ parity) or A_u (− parity) in the I_h point group may exist. Group theoretical analysis (*38*) of the rovibrational wavefunctions shows that this condition is met only with certain linear combinations of k_R states for a given value of R. In fact, only a single such linear combination is possible for R = 0, 6, 10, 12, 15, 16, 18, 20 to 22, and 24 to 28, with other values of $R < 30$ having no allowed states. (For levels with $R \geq 30$, the number of allowed states is equal to 1 plus the number of states for R minus 30.) The unusual patterns of allowed angular momentum quantum numbers are intimately related to the two-, three- and fivefold symmetry axes of an icosahedron. In the high-R limit, only 1 in 60 states exist, owing to the drastic effects of these ^{12}C nuclear spin statistics.

Taking the zeroth-order energies, selection rules, and spin statistics all together leaves the predicted spectrum plotted in black in Fig. 2A. It consists of a sharp Q branch surrounded by P and R branches containing lines evenly spaced by approximately $(B'' + B')(1 - \zeta) \approx 0.0078$ cm^{-1}. The qualitative appearance of the measured R and Q branch regions is consistent with the simulation, whereas there is substantial disagreement in the P branch. The portions of the spectrum shown in Fig. 3 provide a closer view of this behavior.

The R branch exhibits a regularly spaced progression of transitions R(J) that we have assigned from $J \approx 60$ to 360. Transitions outside this range are below our detection sensitivity. Such high values of the total angular momentum quantum number have been rarely observed, if ever, by rotationally resolved frequency domain spectroscopy. Portions of the measured and simulated R branch from J = 160 to 200 are shown in Fig. 3A. Despite the noise in the measured absorption, these transitions clearly show the expected discrete intensity variations in the correct integer ratios. Such patterns are a basic consequence of the quantum mechanical indistinguishability and the perfect icosahedral arrangement of the carbon nuclei that make up $^{12}C_{60}$.

Quantitative analysis of the R branch transition frequencies permits extraction of spectroscopic constants. The energy expressions in Eqs. 2 and 5 yield expected transition frequencies of

$$\begin{aligned} \nu[\mathrm{R}(J)] = \; & \nu_0 + (2\bar{B} + \Delta B)(1 - 2\zeta) + \\ & J[2\bar{B}(1 - \zeta) + \Delta B(2 - \zeta)] + \\ & J^2\Delta B \end{aligned} \quad (6)$$

where $\bar{B} \equiv (B' + B'')/2$ is the mean value of the lower- and upper-state rotational constants and $\Delta B \equiv B' - B'' \ll \bar{B}$ is their difference. Figure 4A shows the measured positions (*34*) as a function of lower state J, which follow the expected nearly linear dependence. Figure 4B shows the residuals from a fit of Eq. 6 to the measured line positions, displaying two avoided crossings arising from perturbations in the excited state. The fitted spectroscopic parameters are summarized in Table 1. The R branch transition frequencies are well reproduced despite the simplicity of the zeroth-order Hamiltonian, which ignores centrifugal distortion effects, and the very high range of J. A complete listing of the ~300 transition frequencies used in this fit is given in data S1 (*39*).

The quantum state–resolved spectrum of C_{60} provides structural information of isolated gas-phase molecules through the rotational fine structure. Although the transitions included in our initial analysis do not yet allow an independent determination of B'' and ζ, if we assume a range of ζ = −0.30 to −0.45 based on theoretical calculations (*37*), we can estimate $B'' = \frac{1}{hc}\frac{\hbar^2}{2I} \approx 0.0027$ to 0.0030 cm^{-1}, where I is the effective moment of inertia of the ground vibrational state, $\hbar$ is Planck's constant h divided by 2π, and c is the speed of light. Given $I = \frac{2}{3}mr^2$ for a spherical shell of mass m and radius r, the corresponding range of radii is 3.4 to 3.6 Å. This is consistent with a previous gas-phase electron diffraction measurement of 3.557(5) Å, which includes thermal averaging effects that lengthen the measured

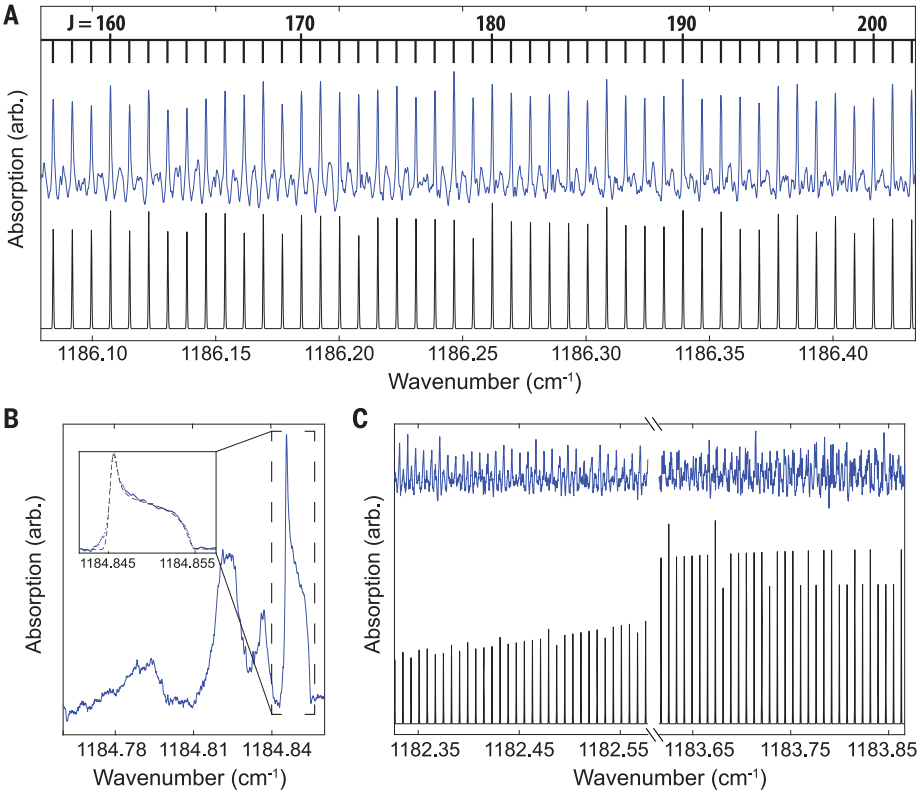

Fig. 3. Detailed views of portions of the measured IR band. (**A**) The R branch shows agreement between the expected intensity patterns from the simulation (black trace) and the measured spectrum (blue trace). The tie line above the spectrum indicates the lower state J value of each observed R(J) transition. (**B**) The Q branch region of the spectrum contains several features. The highest wavenumber feature is assigned as the Q branch of the $^{12}C_{60}$ isotopologue. In the inset, the dashed line represents a fit to a simple quartic centrifugal distortion contour. The additional features at lower frequencies are likely due to the singly substituted $^{13}C^{12}C_{59}$ isotopologue. (**C**) These two portions of the P branch (blue trace) are representative of the disagreement with the zeroth-order simulation determined from parameters fitted to the R branch (black trace). The structure not captured by the simulation is evidence of nonscalar centrifugal distortion effects. arb., arbitrary units.

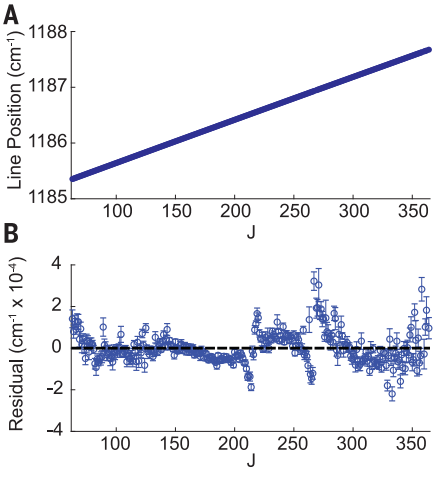

Fig. 4. Fit results for the R branch. (**A**) The R(J) line positions plotted versus lower-state J display a very linear trend over J = 60 to 360. The individual line positions are listed in (*39*). (**B**) The residuals from the fit of Eq. 6 to these line positions, summarized in Table 1, exhibit apparent avoided crossings near J = 215 and 275, which are possible signatures of local dark-state perturbers in the upper state. The error bars are 1σ line-center uncertainties determined from lineshape fit residuals (*34*).

radius relative to that of the vibrational ground state (*8*). Further analysis of the rotational fine structure of $^{12}C_{60}$ (and ultimately $^{12}C_{59}{}^{13}C$) will be necessary to constrain B'' and ζ independently and completely determine the gas-phase structural parameters. Our measured value of ΔB implies that the effective C_{60} radius increases by only 0.005% upon excitation of the observed vibrational mode, which is primarily of a surface-tangent C–C bond stretching character. The narrow IR transition linewidths (about 20 MHz) to the excited vibrational state provide a lower bound for its IVR lifetime of at least 8 ns, despite being embedded in a dense manifold of dark vibrational states. This is consistent with our expectation that the high degree of icosahedral symmetry substantially restricts rovibrational coupling.

The Q branch region is shown in Fig. 3B. There are several unresolved features here, though each is still quite narrow on an absolute scale of 0.01 to 0.03 cm^{-1}. The highest frequency feature is assigned as the Q branch of the $^{12}C_{60}$ isotopologue in its ground vibrational state. Centrifugal distortion effects create a band head observed near J = 250 (inset of Fig. 3B). The remaining features in the Q branch region are not definitively assigned. Although they are possibly hot-band transitions of the $^{12}C_{60}$ isotopologue, we believe they most likely derive from the singly substituted $^{12}C_{59}{}^{13}C$ isotopologue. Despite a ^{13}C natural abundance of only 1.1%, the 60 equivalent substitution sites lead to a notably high ($^{12}C_{59}{}^{13}C$):$^{12}C_{60}$ ratio of about 2:3. The substitution breaks the icosahedral symmetry of C_{60}, splitting the threefold degeneracy of the vibrational level and nullifying the nuclear spin statistics. Many more rotational levels and transitions are expected, which will be further split by the nonspherical moments of inertia (*40*).

Finally, two representative portions of the P branch are shown in Fig. 3C. Here, the zeroth-order simulation fails to capture either the position or number of observed transitions. This complicated fine structure is likely due to high-order centrifugal distortion terms not included in the simulated spectrum (*41*). The zeroth-order Hamiltonians, Eqs. 1 and 3, contain only scalar terms that preserve the spherical degeneracy of the $(2R + 1)$ body-fixed projections of **R**. Whereas most of these substates are eliminated by the ^{12}C nuclear spin statistics, the degeneracy of the remaining substates can be broken by nonscalar centrifugal distortion terms. These so-called "icosahedral splitting" terms (*41*) lead to subsequent splittings of the observed transitions. In the ground state, the lowest-order nonscalar centrifugal distortion term scales as J^6, whereas such terms can appear in the excited state that scale only as J^4. Owing to the large J values observed here, it is not surprising that such effects become important. However, to date, there have been no theoretical predictions of the magnitude of these icosahedral splitting terms. A full analysis of this portion of the spectrum

is most effectively treated within the irreducible spherical tensor formalism (*42*).

The present experiments point toward an exciting future direction of fullerene research. The general applicability of buffer-gas cooling establishes the possibility of similar studies, using vibrational, electronic, or other spectroscopies, on larger fullerenes such as C_{70}; endofullerenes, wherein an atom or small molecule is encapsulated in a closed fullerene cage; or even pure $^{13}C_{60}$, which represents a pristine example of a spin-½ network on a spherical lattice. Ultimately, precision spectroscopy of such targets is the first step toward single quantum state preparation and control of large molecular systems.

REFERENCES AND NOTES

1. H. W. Kroto, J. R. Heath, S. C. O'Brien, R. F. Curl, R. E. Smalley, *Nature* **318**, 162–163 (1985).
2. H. Ajie *et al*., *J. Phys. Chem.* **94**, 8630–8633 (1990).
3. R. Taylor, J. P. Hare, A. K. Abdulsada, H. W. Kroto, *J. Chem. Soc. Chem. Commun.* **1990**, 1423–1424 (1990).
4. W. Krätschmer, K. Fostiropoulos, D. R. Huffman, *Chem. Phys. Lett.* **170**, 167–170 (1990).
5. W. Krätschmer, L. D. Lamb, K. Fostiropoulos, D. R. Huffman, *Nature* **347**, 354–358 (1990).
6. C. S. Yannoni, P. P. Bernier, D. S. Bethune, G. Meijer, J. R. Salem, *J. Am. Chem. Soc.* **113**, 3190–3192 (1991).
7. C. S. Yannoni, R. D. Johnson, G. Meijer, D. S. Bethune, J. R. Salem, *J. Phys. Chem.* **95**, 9–10 (1991).
8. K. Hedberg *et al*., *Science* **254**, 410–412 (1991).
9. S. Liu, Y.-J. Lu, M. M. Kappes, J. A. Ibers, *Science* **254**, 408–410 (1991).
10. S. F. Parker *et al*., *Phys. Chem. Chem. Phys.* **13**, 7789–7804 (2011).
11. L. Pintschovius, *Rep. Prog. Phys.* **59**, 473–510 (1996).
12. D. S. Bethune, G. Meijer, W. C. Tang, H. J. Rosen, *Chem. Phys. Lett.* **174**, 219–222 (1990).
13. D. S. Bethune *et al*., *Chem. Phys. Lett.* **179**, 181–186 (1991).
14. K. Prassides *et al*., *Chem. Phys. Lett.* **187**, 455–458 (1991).
15. R. L. Cappelletti *et al*., *Phys. Rev. Lett.* **66**, 3261–3264 (1991).
16. N. Sogoshi *et al*., *J. Phys. Chem. A* **104**, 3733–3742 (2000).
17. S. Iglesias-Groth, F. Cataldo, A. Manchado, *Mon. Not. R. Astron. Soc.* **413**, 213–222 (2011).
18. A. C. Brieva, R. Gredel, C. Jäger, F. Huisken, T. Henning, *Astrophys. J.* **826**, 122 (2016).
19. X.-B. Wang, C.-F. Ding, L.-S. Wang, *J. Chem. Phys.* **110**, 8217–8220 (1999).
20. D.-L. Huang, P. D. Dau, H.-T. Liu, L.-S. Wang, *J. Chem. Phys.* **140**, 224315 (2014).
21. J. Cami, J. Bernard-Salas, E. Peeters, S. E. Malek, *Science* **329**, 1180–1182 (2010).
22. E. K. Campbell, M. Holz, D. Gerlich, J. P. Maier, *Nature* **523**, 322–323 (2015).
23. D. J. Nesbitt, R. W. Field, *J. Phys. Chem.* **100**, 12735–12756 (1996).
24. D. Patterson, E. Tsikata, J. M. Doyle, *Phys. Chem. Chem. Phys.* **12**, 9736–9741 (2010).
25. J. Piskorski, D. Patterson, S. Eibenberger, J. M. Doyle, *ChemPhysChem* **15**, 3800–3804 (2014).
26. P. B. Changala, B. Spaun, D. Patterson, J. M. Doyle, J. Ye, *Appl. Phys. B* **122**, 292 (2016).
27. B. Spaun *et al*., *Nature* **533**, 517–520 (2016).
28. F. Adler, M. J. Thorpe, K. C. Cossel, J. Ye, *Annu. Rev. Anal. Chem. (Palo Alto, Calif.)* **3**, 175–205 (2010).
29. M. J. Thorpe, J. Ye, *Appl. Phys. B* **91**, 397–414 (2008).
30. K. Iwakuni *et al*., *Appl. Phys. B* **124**, 128 (2018).
31. K. F. Lee, C. J. Hensley, P. G. Schunemann, M. E. Fermann, *Opt. Express* **25**, 17411–17416 (2017).
32. J. Mandon, G. Guelachvili, N. Picqué, *Nat. Photonics* **3**, 99–102 (2009).
33. F. Adler *et al*., *Opt. Express* **18**, 21861–21872 (2010).
34. See supplementary materials.
35. J. T. Stewart, B. E. Brumfield, B. M. Gibson, B. J. McCall, *ISRN Phys. Chem.* **2013**, 675138 (2013).
36. C. di Lauro, in *Rotational Structure in Molecular Infrared Spectra* (Elsevier, 2013), chap. 10, pp. 225–245.
37. D. E. Weeks, W. G. Harter, *Chem. Phys. Lett.* **176**, 209–216 (1991).
38. P. R. Bunker, P. Jensen, *Mol. Phys.* **97**, 255–264 (1999).
39. P. B. Changala, M. L. Weichman, K. F. Lee, M. E. Fermann, J. Ye, External data for "Rovibrational quantum state resolution of the C_{60} fullerene," Version 1, Harvard Dataverse (2018); https://doi.org/10.7910/DVN/RVVAN6.
40. T. C. Reimer, W. G. Harter, *J. Chem. Phys.* **106**, 1326–1335 (1997).
41. W. G. Harter, D. E. Weeks, *J. Chem. Phys.* **90**, 4727–4743 (1989).
42. V. Boudon *et al*., *J. Mol. Spectrosc.* **228**, 620–634 (2004).

ACKNOWLEDGMENTS

The authors thank H. Green for technical advice during the design of the oven source and J. Doyle for insightful discussions. **Funding:** This work was supported by AFOSR grant no. FA9550-15-1-0111, the Gordon and Betty Moore Foundation, the DARPA SCOUT Program, NIST, and NSF PHYS-1734006. M.L.W. is supported through an NRC Postdoctoral Fellowship. **Author contributions:** P.B.C., M.L.W., and J.Y. performed the experiment. K.F.L. and M.E.F. built the DFG-based comb. All authors contributed to the writing of the paper. **Competing interests:** K.F.L. and M.E.F. have submitted a patent (WO2017209989A1) on portions of the DFG frequency comb instrument. **Data and materials availability:** All data are available in the main text, in the supplementary materials, or through Harvard Dataverse (*39*).

SUPPLEMENTARY MATERIALS

www.sciencemag.org/content/363/6422/49/suppl/DC1
Materials and Methods
Fig. S1
References (*43*–*45*)

29 August 2018; accepted 8 November 2018
10.1126/science.aav2616

Science

Rovibrational quantum state resolution of the C_{60} fullerene

P. Bryan Changala, Marissa L. Weichman, Kevin F. Lee, Martin E. Fermann and Jun Ye

Science **363** (6422), 49-54.
DOI: 10.1126/science.aav2616

C_{60} at high resolution

It generally takes more energy for molecules to vibrate than to rotate. A vibrational absorption band thus encompasses many distinct concurrent rotational transitions, but these tend to blur together when the molecules have more than a few atoms. Changala *et al.* succeeded in cooling C_{60} fullerenes sufficiently to obtain rotational resolution within a C–C stretching band. Success hinged on careful optimization of argon buffer gas flow. Such quantum state–resolved features could aid characterization of fullerene-type compounds in exotic environments such as interstellar space.

Science, this issue p. 49